




RESEARCH ARTICLE

Age-related topographic map of magnetic resonance diffusion metrics in neonatal brains

Pratheek S. Bobba¹  | Clara F. Weber^{1,2} | Adrian Mak^{1,3} | Ali Mozayan¹ |
Ajay Malhotra¹ | Kevin N. Sheth⁴ | Sarah N. Taylor⁵ | Arastoo Vossough^{6,7} |
Patricia Ellen Grant^{8,9} | Dustin Scheinost¹  | Robert Todd Constable¹ |
Laura R. Ment^{4,5} | Seyedmehdi Payabvash¹ 

¹Department of Radiology and Biomedical Imaging, Yale School of Medicine, New Haven, Connecticut, USA

²Social Neuroscience Lab, Department of Psychiatry and Psychotherapy, Lübeck University, Lübeck, Germany

³CLAIM - Charité Lab for Artificial Intelligence in Medicine, Charité Universitätsmedizin Berlin, Berlin, Germany

⁴Department of Neurology, Yale University School of Medicine, New Haven, Connecticut, USA

⁵Department of Pediatrics, Yale University School of Medicine, New Haven, Connecticut, USA

⁶Department of Radiology, Children's Hospital of Pennsylvania, Philadelphia, Pennsylvania, USA

⁷Department of Radiology, University of Pennsylvania, Philadelphia, Pennsylvania, USA

⁸Division of Newborn Medicine, Department of Medicine, Boston Children's Hospital, Harvard Medical School, Boston, Massachusetts, USA

⁹Department of Radiology, Boston Children's Hospital, Harvard Medical School, Boston, Massachusetts, USA

Correspondence

Seyedmehdi Payabvash, Department of Radiology and Biomedical Imaging, Yale School of Medicine, 789 Howard Ave, PO Box 208042, New Haven, CT 06519, USA.
Email: sam.payabvash@yale.edu

Funding information

Doris Duke Charitable Foundation, Grant/Award Number: 2020097; National Institute of Diabetes and Digestive and Kidney Diseases of the National Institutes of Health, Grant/Award Number: T35DK104689; National Institutes of Health, Grant/Award Numbers: K23NS101120, K23NS118056, MH111424, MH121095, U24NS107136; American Society of Neuroradiology; Radiological Society of North America, Grant/Award Number: RR2141

Abstract

Accelerated maturation of brain parenchyma close to term-equivalent age leads to rapid changes in diffusion-weighted imaging (DWI) and diffusion tensor imaging (DTI) metrics of neonatal brains, which can complicate the evaluation and interpretation of these scans. In this study, we characterized the topography of age-related evolution of diffusion metrics in neonatal brains. We included 565 neonates who had MRI between 0 and 3 months of age, with no structural or signal abnormality—including 162 who had DTI scans. We analyzed the age-related changes of apparent diffusion coefficient (ADC) values throughout brain and DTI metrics (fractional anisotropy [FA] and mean diffusivity [MD]) along white matter (WM) tracts. Rate of change in ADC, FA, and MD values across 5 mm cubic voxels was calculated. There was significant reduction of ADC and MD values and increase of FA with increasing gestational age (GA) throughout neonates' brain, with the highest temporal rates in subcortical WM, corticospinal tract, cerebellar WM, and vermis. GA at birth had significant effect on ADC values in convexity cortex and corpus callosum as well as FA/MD values in corpus callosum, after correcting for GA at scan. We developed online interactive atlases depicting age-specific normative values of ADC (ages 34–46 weeks), and

Pratheek S. Bobba and Clara F. Weber contributed equally to this study.

This is an open access article under the terms of the [Creative Commons Attribution-NonCommercial-NoDerivs](https://creativecommons.org/licenses/by-nc-nd/4.0/) License, which permits use and distribution in any medium, provided the original work is properly cited, the use is non-commercial and no modifications or adaptations are made.

© 2022 The Authors. *Human Brain Mapping* published by Wiley Periodicals LLC.

FA/MD (35–41 weeks). Our results show a rapid decrease in diffusivity metrics of cerebral/cerebellar WM and vermis in the first few weeks of neonatal age, likely attributable to myelination. In addition, prematurity and low GA at birth may result in lasting delay in corpus callosum myelination and cerebral cortex cellularity.

KEYWORDS

diffusion tensor imaging, diffusion-weighted imaging, magnetic resonance imaging, neonates

1 | INTRODUCTION

Availability of dedicated pediatric coils, lack of radiation exposure, and optimal parenchymal contrast resolution have led to growing utilization of brain magnetic resonance imaging (MRI) in neonates (Oishi et al., 2013). MR diffusion-weighted imaging (DWI) sequences are specialized in the assessment of water molecule diffusibility, which is impacted by tissue cellularity and myelination, allowing this modality to identify pathological conditions such as cytotoxic edema (Cauley & Filippi, 2014; Forkert et al., 2016; Mukherjee et al., 2002). DWI can quantify water diffusion through generation of apparent diffusion coefficient (ADC) maps (Barkovich et al., 2006; Rodrigues & Grant, 2011). Nevertheless, assessment of neonatal brain injury remains particularly challenging as ADC values change rapidly and at varying rates in different regions of the brain during the first few weeks after birth (Coats et al., 2009; Forbes et al., 2002; Zhai et al., 2003). With an increasing number of preterm neonates surviving without any apparent neurodevelopmental and neurostructural abnormality, there is a pressing knowledge gap in characterizing normal topographic and temporal variations of ADC values in neonatal brains.

In addition, diffusion tensor imaging (DTI) can provide greater insight into microstructural properties of brain white matter (WM) by examining the three-dimensional magnitude and direction of water diffusion. Alignment of water molecule along WM axons—as assessed by DTI—is representative of mature myelination and intact fiber tracks (Alexander et al., 2007; Jones & Leemans, 2011). As changes in water diffusion are an early indicator of cellular injury, DTI can also identify subtle injuries of WM (Malavolti et al., 2017; Ward et al., 2006). Indeed, DTI metrics—such as fractional anisotropy (FA) and mean diffusivity (MD)—can delineate both normal and abnormal microstructural development in neonatal brains (Hüppi et al., 1998; McGraw et al., 2002; Zhai et al., 2003). However, interpretation of neonatal DTI scans is also challenging due to rapid temporal changes of FA and MD values in the first few weeks after birth, and limited number of studies describing the normative range in neonatal DTI metrics (Neil et al., 1998; Neil et al., 2002; Schneider et al., 2004).

In current study, we characterized the topology of age-related alterations in diffusion MRI metrics (ADC, FA, and MD) in neonatal brains using a large cohort with no apparent neurological deficit or imaging abnormality. We also determined the location-specific rate of changes in ADC, FA, and MD values. Then, we generated and publicly

shared an age-adjusted normative atlas of diffusion MRI metrics in neonatal brains (<https://www.brain-diffusion-atlas.com>).

2 | METHODS

2.1 | Subjects

In this retrospective study, the records of all neonates who had brain MRI between January 2013 and March 2021 within 3 months of birth at Yale New Haven Hospital were reviewed. At our institution, preterm neonates generally undergo brain MRI before discharge to exclude any potential cerebral abnormality. We included neonates who had (1) normal brain MRI based on clinical report and visually confirmed by a neuroradiologist with over 10 years of experience; (2) optimal quality DWI series without artifact; and (3) reliable history to ascertain the gestational age (GA) at birth and scan time. For a subset of neonates who could tolerate MRI and remained still during scans, additional DTI scans were obtained as part of the clinical imaging protocol. These neonates were included for analysis of FA and MD metrics. We limited our analysis to the age range where imaging data were available for ≥ 10 neonates per week GA at the time of scan: 34–46 weeks for DWI and 35–41 weeks for DTI analysis. Our study design was approved by the institutional review board.

2.2 | Image acquisition

MRIs were performed on a Siemens 3 T Skyra scanner. Axial DWIs were obtained using a single-shot echoplanar imaging sequence: TR = 6500 ms, TE = 90 ms, Flip angle = 90, field of view 22×22 cm, slice thickness of 4 mm, matrix of 130×130 , and b-values of 0, 500, and 1000 s/mm². Axial DTIs were obtained using a single-shot echoplanar imaging sequence: TR = 10,200 ms, TE = 94 ms, Flip angle = 90, field of view 18×18 cm, slice thickness of 2.5 mm, matrix of 128×128 , including a single b=0 and 30 noncolinear direction b=1000 s/mm² acquisitions.

2.3 | Image preprocessing

We used the FDT toolbox in FSL for processing of DTI scans and to generate FA and MD maps (Payabvash et al., 2019; Payabvash

et al., 2019a, 2019b). The FLIRT function in the FSL software was then used to co-register DWI scans (and associated ADC maps) to a pediatric brain template generated from MRI scans of patients between 0 and 2 years of age (<http://nist.mni.mcgill.ca/infant-atlases-0-4-5-years/>) (Fonov et al., 2011; Payabvash et al., 2019; Payabvash et al., 2019a, 2019b). FA (and corresponding MD) maps were co-registered to the pediatric brain template by first co-registering these scans to the corresponding subject's DWI scan and then using the co-registration matrices from the DWI co-registration process to bring the FA and MD maps to the same space as the pediatric brain template. All co-registered scans were again visually inspected for quality control.

2.4 | Voxel-wise general linear model analysis

We used the “randomize” tool in FSL for voxel-wise general linear model (GLM) analysis of age-related changes in ADC, FA, and MD values (Payabvash et al., 2019; Payabvash et al., 2019a, 2019b). We applied 5000 permutations and threshold-free cluster enhancement while correcting for multiple comparisons. A color-coded map of p values was generated, windowed for p values between 0 and .05, and overlaid onto the pediatric brain template (Fonov et al., 2011). Additional analyses were conducted to analyze the correlation between GA at birth and diffusion metrics, after correcting for GA at time of scan as a covariate.

2.5 | Voxel-wise tract-based spatial statistics

We used the TBSS toolbox in FSL to conduct voxel-wise statistical analysis of FA and MD values along the WM tracts (Smith et al., 2006). Using TBSS, the most representative FA map of the DTI subset was identified by co-registering each FA map to all other FA maps. This target image was then co-registered to the pediatric brain template and the rest of the FA maps were co-registered to the pediatric brain template by combining the registration to the target and the registration from the target to the standardized MNI-152 brain space (Payabvash et al., 2019; Payabvash et al., 2019a, 2019b). These newly aligned FA maps were averaged to generate a skeletonized WM tract across all neonates followed by application of a threshold value of 0.1. The aligned FA maps and skeletonized WM tracts were then co-registered to the pediatric brain template prior to further analysis (Fonov et al., 2011). Then, we applied “randomize” with 5000 permutations and threshold-free cluster enhancement for voxel-wise GLM analysis of FA, and MD values across WM tracts.

2.6 | Tract-specific analysis of DTI metrics

Using merged images from the TBSS operation and a Johns Hopkins University atlas that was co-registered to the pediatric brain template, the means of non-zero FA and MD values in each of 48 WM tract

regions were calculated for each subject (Fonov et al., 2011; Payabvash et al., 2019a). We then applied multiple linear regressions to analyze the impact of both GA at scan and GA at birth on mean FA and MD values in each of these 48 WM tracts.

2.7 | Mapping the rate of age-related alterations in diffusion metrics

A series of isotropic $5 \times 5 \times 5$ mm voxels were generated in the pediatric brain template space after eroding a 2-mm edge off from a mask generated from the pediatric brain template using a spherical kernel, resulting in 5539 cubic regions of interests (ROIs) (Fonov et al., 2011). These ROIs were then reverse co-registered to native DWI and DTI spaces of each subject using the reverse co-registration matrices from the aforementioned co-registration processes. For reverse co-registering the ROIs to the DTI masks using two reverse-co-registration matrices, a threshold value of 0.5 was applied before binarizing the final ROIs to prevent overlap of multiple ROIs in a given voxel in the native space of each subject. We also applied each subject's DWI scan as a mask to exclude any potential CSF space. Next, we calculated the average of non-zero ADC, FA, and MD values in each ROI for every neonate. Applying linear regression, we calculated the slope of age-related changes in the average ADC, FA, and MD values for each ROI across all subjects. The slope of age-related decline in ADC and MD and increase in FA was then mapped to the pediatric brain template and then smoothed by mean filtering with a Gaussian kernel of 3 mm (Fonov et al., 2011).

2.8 | Normative map of neonatal brain diffusion metrics per gestational age

Subjects were grouped according to GA at scan week with those aged between two gestational weeks assigned to the lower week—for example, neonates born between 35 weeks and 0 days to 35 weeks and 6 days were grouped in a cohort denoted as 35 weeks of GA. For each ROI, the average and standard deviation of the ADC, FA, and MD values were calculated across all neonates belonging to each GA cohort. These values were then used to generate an online age-adjusted normative map of diffusion MRI metrics (<https://www.brain-diffusion-atlas.com>). Values of selected metrics are visualized by creating a vertical scatter plot by “gestational age at scan in weeks,” with error bars reflecting the standard deviation.

2.9 | Statistics

The data are expressed as mean \pm standard deviation, median (interquartile [IQR]), or frequency (percentage) as appropriate. The “stats” package in R was used for linear regression analysis and for the generation of age-adjusted normative maps.

3 | RESULTS

3.1 | Neonates' characteristics

We identified 1775 unique neonates who had MRI with DWI sequence within 3 months of birth. Of these, 565 neonates met our inclusion criteria for DWI and 162 for DTI analysis (Figure 1). Table 1 summarizes the demographic characteristics of neonates included in DWI/ADC and DTI analyses. Figure 2 displays the histogram distributions of GA at scan for subjects in the DWI/ADC and DTI cohorts.

3.2 | Age-related changes in cerebral ADC and WM tract DTI metrics

On voxel-wise GLM analysis of ADC values, there was pervasive significant reduction in ADC with increasing GA at the time of scan (Figure S1A). In TBSS analysis of DTI metrics, there was significant age-related increase in FA (Figure 3a) and decrease in MD (Figure 3b) of bilateral superior longitudinal fasciculus, corpus callosum, corticospinal tracts (from corona radiata, through internal capsule, and into the brainstem), and external capsule.

3.3 | Topographic rate of age-related changes in neonatal brain diffusion metrics

Figure 4 displays the rates of decline in ADC and MD, and rise in FA values with increasing GA at scan time in neonatal brain. Rates of decline in ADC values ranged from $-0.028 \times 10^{-6} \text{ mm}^2/\text{s}$ to $-59.64 \times 10^{-6} \text{ mm}^2/\text{s}$ per week, with the highest rates of decline with increasing GA in the frontal/parietal/occipital subcortical WM, centrum semiovale, cerebellar WM and vermis (Figure 4a). Rates of

increase in FA values ranged from 0.0001×10^{-2} to 1.8×10^{-2} per week, with the highest rates of increase with increasing GA at scan time in the subcortical WM, and corticospinal tract (Figure 4b). Rates of decline in MD values ranged from $-0.01 \times 10^{-4} \text{ mm}^2/\text{s}$ to $-0.95 \times 10^{-4} \text{ mm}^2/\text{s}$ per week, with the highest rates of decline with increasing GA at scan time in the juxtacortical WM of frontal/parietal lobes as well as cerebellar WM and vermis (Figure 4c).

3.4 | The effects of GA at birth on diffusion metrics at the time of scan

Figure S1B displays the results of voxel-wise GLM analysis, evaluating the effects of GA at birth on ADC values after correcting for age at scan time. Higher GA at birth (more mature neonate) is associated

TABLE 1 Neonate characteristics

Characteristics	DWI/ADC cohort (n = 565)	DTI cohort (n = 162) ^a
Week gestational age at scan (mean ± SD)	39.68 ± 2.79	38.53 ± 1.94
Week gestational age at birth (mean ± SD)	34.50 ± 5.52	32.52 ± 5.71
1 min APGAR score (median [IQR])	7 (4–9)	6 (4–8)
5 min APGAR score (median [IQR])	9 (7–9)	8 (7–9)
Percentage of males	52.4%	60.4%

Note: All 162 subjects were used for all other DTI cohort analyses. Abbreviations: ADC, apparent diffusion coefficient; DWI, diffusion-weighted imaging; DTI, diffusion tensor imaging.

^aThree subjects were excluded prior to tract based spatial statistics (TBSS) analysis due to TBSS co-registration failure.

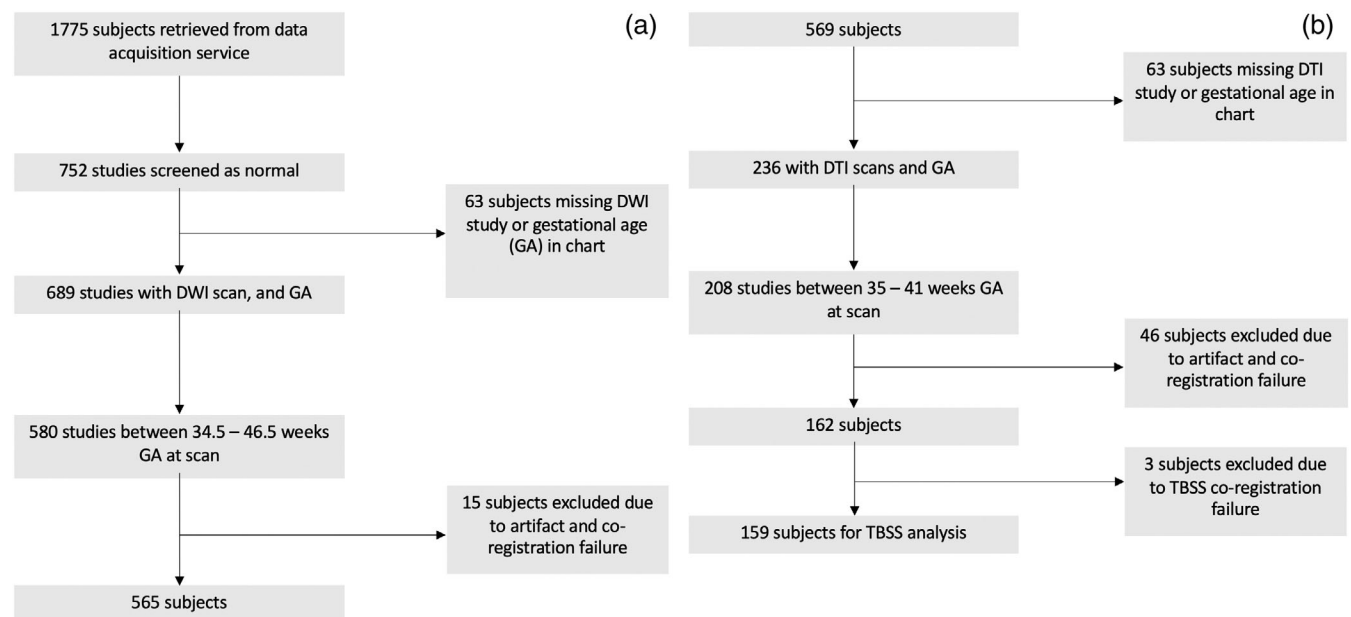


FIGURE 1 Neonate inclusion flowchart for (a) apparent diffusion coefficient (ADC) and (b) diffusion tensor imaging (DTI) metrics analysis

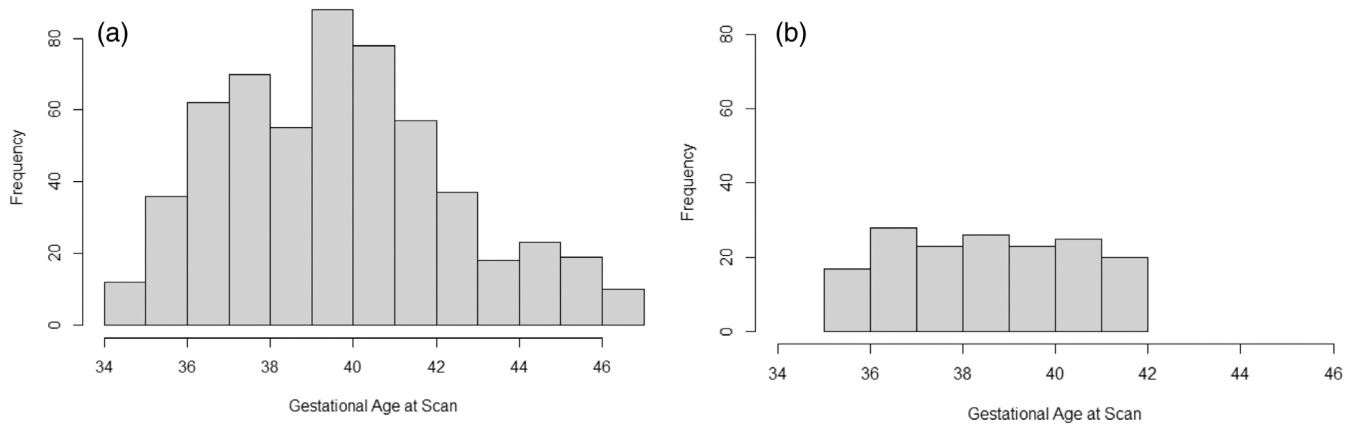


FIGURE 2 Histogram displaying gestational age at scan distribution for (a) diffusion-weighted imaging (DWI) cohort and (b) diffusion tensor imaging (DTI) cohort

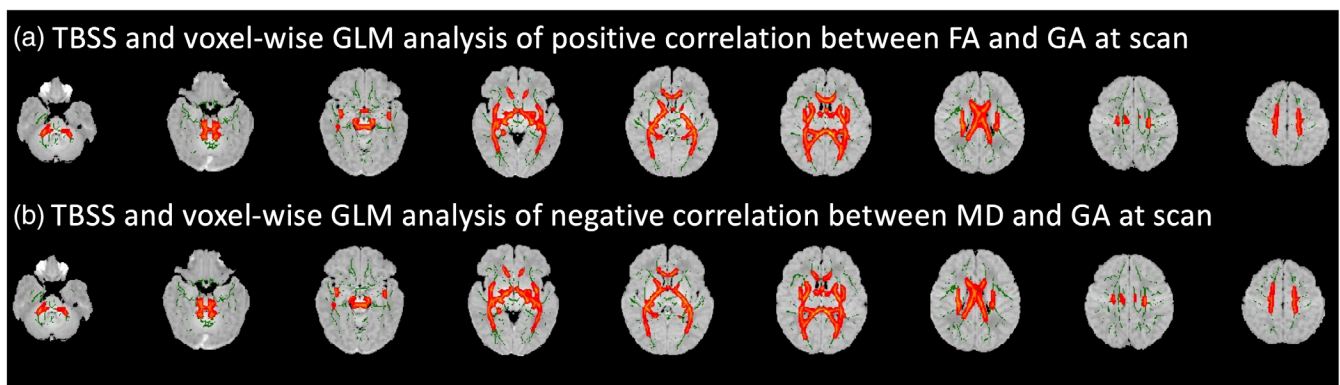


FIGURE 3 Tract-based spatial statistics (TBSS) and general linear model (GLM) analysis of (a) significant increase in fractional anisotropy (FA) and (b) decline in mean diffusivity (MD) in white matter tracts, when assessing the influence of increasing gestational age (GA) at the time of scan. Green areas display the estimated white matter tract FA skeleton; red areas depict sites where high GA at scan had a significant impact on FA or MD values ($p < .05$).

with lower ADC in the corpus callosum as well as the convexity cortex after correcting for GA at scan time as a covariate. Figure 5 depicts the results of TBSS analysis, evaluating the effects of GA at birth on DTI metrics of WM tracts after correcting for age at scan time. Higher GA at birth (more mature neonate) is associated with higher FA (Figure 5a) and lower MD (Figure 5b) values in the corpus callosum and to lesser extent in the corticospinal tract after correcting for GA at scan time as a covariate. Tract-specific analysis confirmed the results of voxel-wise analysis for independent effects of GA at birth on FA and MD values in the corpus callosum, posterior thalamic radiation, cingulate gyrus, and superior longitudinal fasciculus (Tables S1 and S2).

3.5 | An online interactive atlas of age-specific diffusion metrics for the neonatal brain

We calculated the mean \pm SD of ADC, FA, and MD values for each 5 mm cubic isotropic voxel in neonates' brains belonging to the same

week of GA at scan time. Figure 6 shows a sample image of the online interactive atlas (<https://www.brain-diffusion-atlas.com>). Users can choose a diffusion MRI metric (ADC, FA or MD), scroll through the representative ADC map, and view a plot displaying the age-specific diffusion metrics by clicking on each voxel. By hovering the mouse cursor over specific plot points, users can view the mean \pm SD of the diffusion metric for a specific GA at scan time as well as the sample size of neonates contributing to the calculations in that particular GA cohort. Plots can also be re-sized by dragging a box over a particular region of the plot and reset to original size.

4 | DISCUSSION

In this study, we found widespread decline in brain ADC values with increasing age of neonates at the time of scan, which is mostly related to maturation/myelination of WM tracts as DTI analysis shows that the highest rates of age-related decline in ADC topographically correspond to areas of the fastest FA increase and MD decrease. When

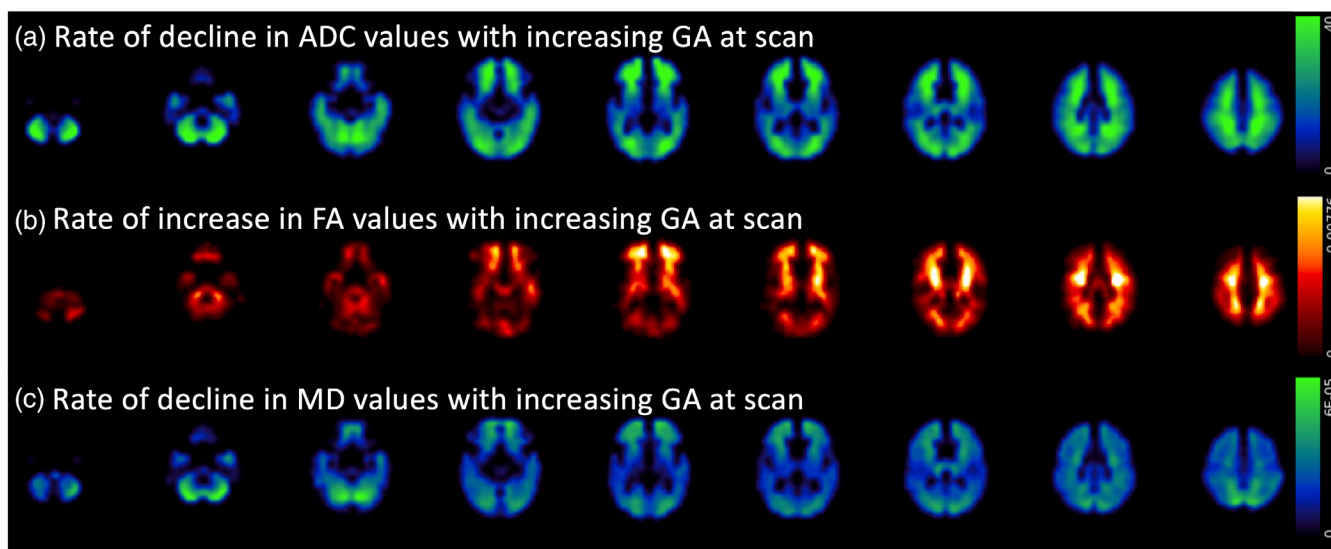


FIGURE 4 Topology of age-related decline in apparent diffusion coefficient (ADC) and mean diffusivity (MD) values and increase in fractional anisotropy (FA). Color bars display the slope values derived from linear regression analysis between gestational age (GA) at the scan time and diffusion metrics at each 5 mm isotropic voxel. (a) The rate of decline in ADC values with increasing GA at scan. Values are negated, with higher intensities representing faster rates of decline. Color bar values are expressed in $\times 10^{-6}$ mm²/s; (b) the rate of increase in FA values with increasing gestational age at the time of scan. Higher intensities represent faster rates of increase; (c) the rate of decline in MD values with increasing gestational age at the time of scan. Values are negated, with higher intensities representing faster rates of decline. Color bar values are expressed in mm²/s.

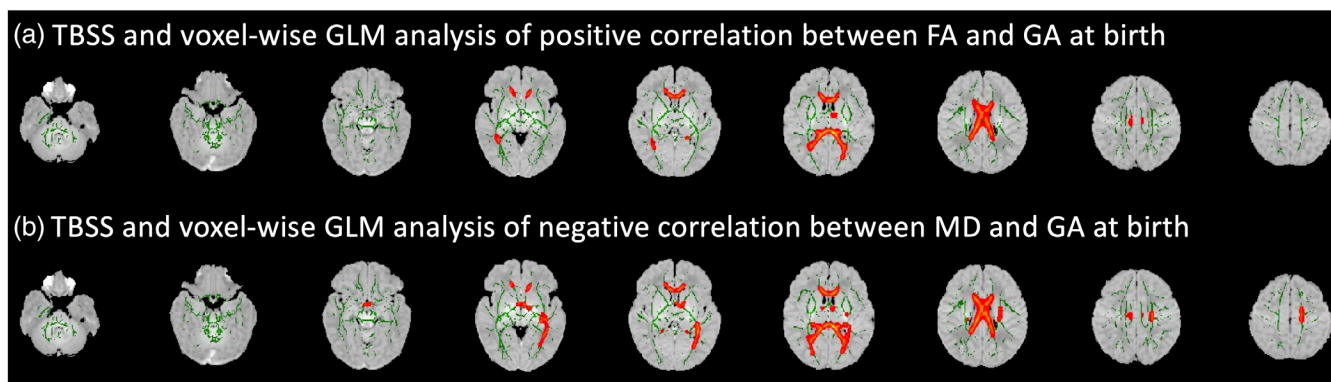


FIGURE 5 Tract-based spatial statistics (TBSS) and general linear model (GLM) analysis showing areas of (a) higher fractional anisotropy (FA) and (b) lower mean diffusivity (MD) values with increasing gestational age (GA) at birth independent of gestational age at the time of scan. Green areas display the estimated white matter tract FA skeleton; red areas depict sites where increasing GA at birth had a significant impact on FA or MD values ($p < .05$).

analyzing the impact of GA at birth on diffusion metrics at the time of scan, we found that higher GA (more mature neonates) tends to be associated with lower ADC in the convexity cortex and the corpus callosum (after correction for GA at scan time). Similarly, we found higher FA and lower MD values in the corpus callosum of more mature neonates at birth after correction for the GA at the time of scan. These findings localize brain regions where lower GA at birth may lead to enduring delay in maturation of WM tracts and perhaps cortex cellularity. On the other hand, diffusion metrics in those areas of the brain not significantly impacted by the GA at birth (Figure S1B and Figure 5) are predominantly determined by the GA at the time of scan.

Thus, a normative atlas of age-specific diffusion metrics would be most generalizable in these regions (regardless of the neonatal age at birth) and can help identify subtle metabolic/toxic brain injuries in neonates.

Our study elucidates the potential neurobiology of age-related changes in diffusion metrics of the brain in the earliest weeks of neonatal growth by determining the temporal rate of changes in diffusion MRI metrics in neonatal brains. Previous studies support our results reporting an increase in FA and decrease in diffusivity (ADC and MD) with increasing GA (McGraw et al., 2002; Neil et al., 2002; Oishi et al., 2013). Notably, these changes in DTI metrics have been linked

Age-specific map of diffusion metrics in the neonate brain. The data are driven from 565 neonates for DWI/ADC maps, and 162 for DTI metrics. All neonates were neurologically and radiologically normal.

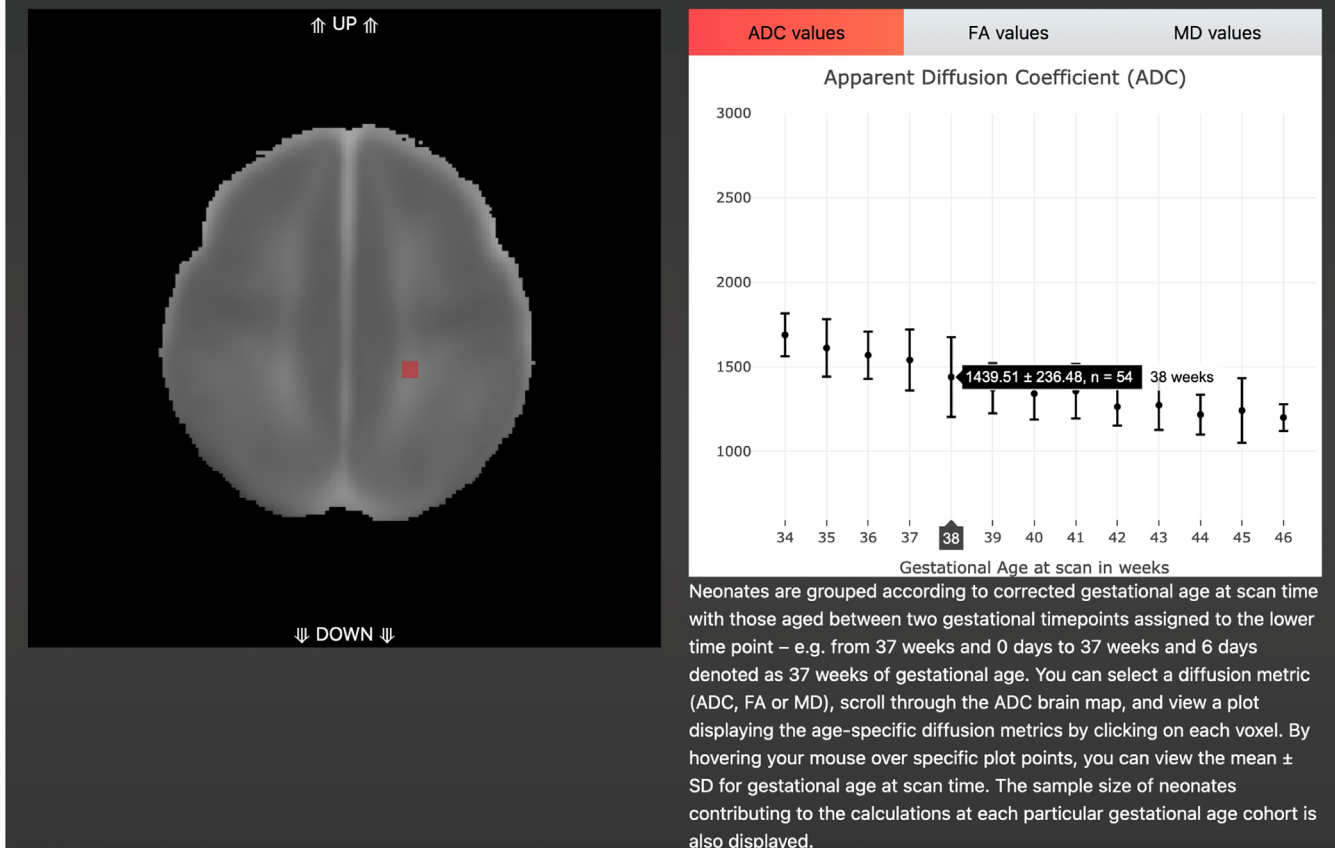


FIGURE 6 An online normative atlas of age-specific diffusion metrics in neonatal brains (<https://www.brain-diffusion-atlas.com>). The users can scroll through a representative apparent diffusion coefficient (ADC) scan and click on any location (5 mm isotropic voxel) to generate a plot displaying the mean \pm standard deviation of ADC (currently selected), fractional anisotropy (FA) or mean diffusivity (MD) values for different gestational age at the time of scan, in the selected voxel (red square). Hovering over a plot point will depict additional information about the sample size of neonates that contributed to the measurement at that particular week of gestational age.

to the myelination of WM and increased cellularity of gray matter, both of which contribute to reduction in water content of the neonatal brain tissue (Forkert et al., 2016; Hüppi et al., 1998; Mukherjee et al., 2002; Schneider et al., 2004). Thus, we proposed that the higher temporal rate of age-related decrease in ADC values along the WM tract is primarily due to myelination, whereas the lower temporal rate of age-related decrease in ADC within the cortex and basal ganglia is due to increase in cellularity.

In addition, we showed that the GA at birth predominantly affects the ADC values in the convexity cortex as well as the corpus callosum and to lesser extent the superior longitudinal fasciculus after correction for GA at scan time as a covariate. The association of higher GA at birth with lower ADC/MD and higher FA in the corpus callosum and select WM tracts are suggestive of a region-specific vulnerability of myelination and microstructural development to preterm delivery. Such areas may be more vulnerable to developmental delay by prematurity (Figure 5 and Figure S1B), whereas the rest of WM may develop/myelinate (normally) despite prematurity (Dudink

et al., 2007; Rose et al., 2014). These findings can also denote brain regions where our age-specific normative atlas for diffusion metrics is generalizable regardless of neonate's age at birth.

Multiple studies have reported an added value from quantitative analysis of ADC maps for detecting neonatal hypoxic ischemic encephalopathy (HIE) when compared to visual qualitative assessment (Cauley & Filippi, 2014; Wolf et al., 2001). Quantitative assessment of ADC values in neonatal brain is, however, challenging due to rapid decline with increasing GA, which varies in different cerebral regions (Forbes et al., 2002; Neil et al., 1998; Zhai et al., 2003). For example, while prior reports agree that changes in ADC values in posterior limb of the internal capsule can identify and predict outcomes in neonatal HIE, they differ in the topology of other cerebral regions implicated in HIE injury (Coats et al., 2009; Liauw et al., 2009; Wolf et al., 2001). These discrepancies and lack of standardized ADC values across the neonatal brain reflect the gap for a normative age-adjusted atlas. Prior attempts for generation of such atlas were limited by low sample sizes, focus on too narrow of an age window, or lack of organized age

group stratification (Feng et al., 2019; Geng et al., 2012). Our atlas addresses these concerns and is strengthened by using a large number of radiologically normative neonates ($n = 565$) across a wider range of GAs (not just term equivalent) and by grouping subjects by GA at scan week. In addition, we utilized a dedicated pediatric brain template for co-registration and voxel wise analysis. Our online atlas can help radiologists with quantitative assessment of ADC maps and detection of visually subtle forms of parenchymal injury.

Several prior studies also described the utility of DTI metrics in identifying WM injuries—including HIE—in neonates (Malavolti et al., 2017; Malik et al., 2006; Tusor et al., 2012). However, as with ADC maps, the age-related and region-specific differences in DTI metrics can complicate the identification of WM injury on DTI scans (Brissaud et al., 2010; Lemmon et al., 2017). There is also relatively scarce prior reports on normative DTI metric values in neonatal brains. Our FA and MD maps seek to fill these gaps and provide age-specific normative reference values to facilitate the application of DTI scans for identification of WM injuries or developmental abnormalities in neonates. We provide additional novelty over previous studies by characterizing the topographic temporal rate of diffusion metrics evolution in neonates' brains.

Our study is limited by a retrospective and single center design. In addition, the sample size in the DTI subset is smaller compared to the DWI/ADC cohort. Generalizability of ADC values is also restricted based on scanner magnet power and acquisition technique. However, prior studies suggest that applying similar scan parameters can minimize such variability (Belli et al., 2016; Huo et al., 2016). Similarly, DTI metrics can be affected by acquisition protocol as well as computation method in generation of final metrics map. Additionally, we acknowledge that the slice thickness used in the acquisition of DWI and DTI scans is relatively large given the small size of a neonatal brain. Thinner slices and smaller voxel size can improve the resolution of final images and quantitative maps.

Through analysis of DWI ($n = 565$) and DTI ($n = 162$) scans in radiologically normal neonates, we mapped the age-related changes of diffusion MRI metrics and developed interactive atlases depicting the normative ranges for different GAs at scan time. The age-related evolution of ADC values and DTI metrics were most pronounced in WM tracts, likely representing fast myelination in these areas. Notably, diffusion metrics in the cortex and corpus callosum are affected by the GA at birth, which may reflect lasting delay in maturation/myelination of these regions due to preterm birth. Considering these limitations, we publicly share age-adjusted diffusion atlases to facilitate the quantitative assessment of DWI and DTI scans for detection of developmental abnormalities or parenchymal injuries in neonates.

ACKNOWLEDGMENTS

None.

FUNDING INFORMATION

Pratheek S. Bobba received support from the National Institute of Diabetes and Digestive and Kidney Diseases of the National Institutes

of Health (T35DK104689). Ali Mozayan received support from Radiological Society of North America (RR2141). Kevin Sheth received support from the NIH (U24NS107136). Patricia Ellen Grant received support from National Institutes of Health (K23NS101120). Todd Constable received support from National Institutes of Health Grants MH111424 and MH121095. Seyedmehdi Payabvash received grant support from National Institutes of Health (K23NS118056), Doris Duke Charitable Foundation (2020097) and Foundation of American Society of Neuroradiology.

CONFLICT OF INTEREST

The authors declare no conflicts of interest.

DATA AVAILABILITY STATEMENT

Data generated or analyzed during the study are available from the corresponding author by request.

ETHICS STATEMENT

Our study design was reviewed and approved by the institutional review board.

ORCID

Pratheek S. Bobba  <https://orcid.org/0000-0003-4255-301X>

Dustin Scheinost  <https://orcid.org/0000-0002-6301-1167>

Seyedmehdi Payabvash  <https://orcid.org/0000-0003-4628-0370>

REFERENCES

- Alexander, A. L., Lee, J. E., Lazar, M., & Field, A. S. (2007). Diffusion tensor imaging of the brain. *Neurotherapeutics*, 4(3), 316–329.
- Barkovich, A. J., Miller, S., Bartha, A., Newton, N., Hamrick, S., Mukherjee, P., Glenn, O., Xu, D., Partridge, J., & Ferriero, D. (2006). MR imaging, MR spectroscopy, and diffusion tensor imaging of sequential studies in neonates with encephalopathy. *American Journal of Neuroradiology*, 27(3), 533–547.
- Belli, G., Busoni, S., Ciccarone, A., Coniglio, A., Esposito, M., Giannelli, M., Mazzoni, L. N., Nocetti, L., Sghedoni, R., & Tarducci, R. (2016). Quality assurance multicenter comparison of different MR scanners for quantitative diffusion-weighted imaging. *Journal of Magnetic Resonance Imaging*, 43(1), 213–219.
- Brissaud, O., Amirault, M., Villella, F., Periot, O., Chateil, J., & Allard, M. (2010). Efficiency of fractional anisotropy and apparent diffusion coefficient on diffusion tensor imaging in prognosis of neonates with hypoxic-ischemic encephalopathy: A methodologic prospective pilot study. *American Journal of Neuroradiology*, 31(2), 282–287.
- Cauley, K. A., & Filippi, C. G. (2014). Apparent diffusion coefficient histogram analysis of neonatal hypoxic-ischemic encephalopathy. *Pediatric Radiology*, 44(6), 738–746.
- Coats, J. S., Freeberg, A., Pajela, E. G., Obenaus, A., & Ashwal, S. (2009). Meta-analysis of apparent diffusion coefficients in the newborn brain. *Pediatric Neurology*, 41(4), 263–274.
- Dudink, J., Lequin, M., van Pul, C., Buijs, J., Conneman, N., van Goudoever, J., & Govaert, P. (2007). Fractional anisotropy in white matter tracts of very-low-birth-weight infants. *Pediatric Radiology*, 37(12), 1216–1223.
- Feng, L., Li, H., Oishi, K., Mishra, V., Song, L., Peng, Q., Ouyang, M., Wang, J., Slinger, M., Jeon, T., Lee, L., Heyne, R., Chalak, L., Peng, Y., Liu, S., & Huang, H. (2019). Age-specific gray and white matter DTI atlas for human brain at 33, 36 and 39 postmenstrual weeks. *NeuroImage*, 185, 685–698.

- Fonov, V., Evans, A. C., Botteron, K., Almli, C. R., McKinstry, R. C., & Collins, D. L. (2011). Unbiased average age-appropriate atlases for pediatric studies. *NeuroImage*, 54(1), 313–327.
- Forbes, K. P. N., Pipe, J. G., & Bird, C. R. (2002). Changes in brain water diffusion during the 1st year of life. *Radiology*, 222(2), 405–409.
- Forkert, N. D., Li, M. D., Lober, R. M., & Yeom, K. W. (2016). Gray matter growth is accompanied by increasing blood flow and decreasing apparent diffusion coefficient during childhood. *American Journal of Neuroradiology*, 37(9), 1738–1744.
- Geng, X., Gouttard, S., Sharma, A., Gu, H., Styner, M., Lin, W., Gerig, G., & Gilmore, J. H. (2012). Quantitative tract-based white matter development from birth to age 2 years. *NeuroImage*, 61(3), 542–557.
- Huo, J., Alger, J., Kim, H., Brown, M., Okada, K., Pope, W., & Goldin, J. (2016). Between-scanner and between-visit variation in normal white matter apparent diffusion coefficient values in the setting of a multi-center clinical trial. *Clinical Neuroradiology*, 26(4), 423–430.
- Hüppi, P. S., Maier, S. E., Peled, S., Zientara, G. P., Barnes, P. D., Jolesz, F. A., & Volpe, J. J. (1998). Microstructural development of human newborn cerebral white matter assessed in vivo by diffusion tensor magnetic resonance imaging. *Pediatric Research*, 44(4), 584–590.
- Jones, D. K., & Leemans, A. (2011). Diffusion tensor imaging. In *Magnetic resonance neuroimaging* (pp. 127–144). Springer.
- Lemmon, M. E., Wagner, M. W., Bosemani, T., Carson, K. A., Northington, F. J., Huisman, T. A., & Poretti, A. (2017). Diffusion tensor imaging detects occult cerebellar injury in severe neonatal hypoxic-ischemic encephalopathy. *Developmental Neuroscience*, 39(1–4), 207–214.
- Liauw, L., van Wezel-Meijler, G., Veen, S., Van Buchem, M., & van der Grond, J. (2009). Do apparent diffusion coefficient measurements predict outcome in children with neonatal hypoxic-ischemic encephalopathy? *American Journal of Neuroradiology*, 30(2), 264–270.
- Malavolti, A. M., Chau, V., Brown-Lum, M., Poskitt, K. J., Brant, R., Synnes, A., Grunau, R. E., & Miller, S. P. (2017). Association between corpus callosum development on magnetic resonance imaging and diffusion tensor imaging, and neurodevelopmental outcome in neonates born very preterm. *Developmental Medicine & Child Neurology*, 59(4), 433–440.
- Malik, G., Trivedi, R., Gupta, R., Hasan, K., Hasan, M., Gupta, A., Pandey, C., & Narayana, P. (2006). Serial quantitative diffusion tensor MRI of the term neonates with hypoxic-ischemic encephalopathy (HIE). *Neuropediatrics*, 37(06), 337–343.
- McGraw, P., Liang, L., & Provenzale, J. M. (2002). Evaluation of normal age-related changes in anisotropy during infancy and childhood as shown by diffusion tensor imaging. *American Journal of Roentgenology*, 179(6), 1515–1522.
- Mukherjee, P., Miller, J. H., Shimony, J. S., Philip, J. V., Nehra, D., Snyder, A. Z., Conturo, T. E., Neil, J. J., & McKinstry, R. C. (2002). Diffusion-tensor MR imaging of gray and white matter development during Normal human brain maturation. *American Journal of Neuroradiology*, 23(9), 1445–1456.
- Neil, J., Miller, J., Mukherjee, P., & Hüppi, P. S. (2002). Diffusion tensor imaging of normal and injured developing human brain—a technical review. *NMR in Biomedicine: An International Journal Devoted to the Development and Application of Magnetic Resonance In Vivo*, 15(7–8), 543–552.
- Neil, J. J., Shiran, S. I., McKinstry, R. C., Scheff, G. L., Snyder, A. Z., Almli, C. R., Akbudak, E., Aronovitz, J. A., Miller, J. P., & Lee, B. (1998). Normal brain in human newborns: Apparent diffusion coefficient and diffusion anisotropy measured by using diffusion tensor MR imaging. *Radiology*, 209(1), 57–66.
- Oishi, K., Faria, A. V., Yoshida, S., Chang, L., & Mori, S. (2013). Quantitative evaluation of brain development using anatomical MRI and diffusion tensor imaging. *International Journal of Developmental Neuroscience*, 31(7), 512–524.
- Payabvash, S., Palacios, E. M., Owen, J. P., Wang, M. B., Tavassoli, T., Gerdes, M., Brandes-Aitken, A., Cuneo, D., Marco, E. J., & Mukherjee, P. (2019). White matter connectome edge density in children with autism spectrum disorders: Potential imaging biomarkers using machine-learning models. *Brain Connectivity*, 9(2), 209–220.
- Payabvash, S., Palacios, E. M., Owen, J. P., Wang, M. B., Tavassoli, T., Gerdes, M., Brandes-Aitken, A., Marco, E. J., & Mukherjee, P. (2019a). Diffusion tensor tractography in children with sensory processing disorder: Potentials for devising machine learning classifiers. *NeuroImage Clinical*, 23, 101831.
- Payabvash, S., Palacios, E. M., Owen, J. P., Wang, M. B., Tavassoli, T., Gerdes, M., Brandes-Aitken, A., Mukherjee, P., & Marco, E. J. (2019b). White matter connectome correlates of auditory over-responsivity: Edge density imaging and machine-learning classifiers. *Frontiers in Integrative Neuroscience*, 13, 10.
- Rodrigues, K., & Grant, P. E. (2011). Diffusion-weighted imaging in neonates. *Neuroimaging Clinics*, 21(1), 127–151.
- Rose, J., Vassar, R., Cahill-Rowley, K., Stecher Guzman, X., Hintz, S. R., Stevenson, D. K., & Barnea-Goraly, N. (2014). Neonatal physiological correlates of near-term brain development on MRI and DTI in very-low-birth-weight preterm infants. *NeuroImage: Clinical*, 5, 169–177.
- Schneider, J. F. L., Il'yasov, K. A., Hennig, J., & Martin, E. (2004). Fast quantitative diffusion-tensor imaging of cerebral white matter from the neonatal period to adolescence. *Neuroradiology*, 46(4), 258–266.
- Smith, S. M., Jenkinson, M., Johansen-Berg, H., Rueckert, D., Nichols, T. E., Mackay, C. E., Watkins, K. E., Ciccarelli, O., Cader, M. Z., Matthews, P. M., & Behrens, T. E. (2006). Tract-based spatial statistics: Voxelwise analysis of multi-subject diffusion data. *NeuroImage*, 31(4), 1487–1505.
- Tusor, N., Wusthoff, C., Smee, N., Merchant, N., Arichi, T., Allsop, J. M., Cowan, F. M., Azzopardi, D., Edwards, A. D., & Counsell, S. J. (2012). Prediction of neurodevelopmental outcome after hypoxic-ischemic encephalopathy treated with hypothermia by diffusion tensor imaging analyzed using tract-based spatial statistics. *Pediatric Research*, 72(1), 63–69.
- Ward, P., Counsell, S., Allsop, J., Cowan, F., Shen, Y., Edwards, D., & Rutherford, M. (2006). Reduced fractional anisotropy on diffusion tensor magnetic resonance imaging after hypoxic-ischemic encephalopathy. *Pediatrics*, 117(4), e619–e630.
- Wolf, R. L., Zimmerman, R. A., Clancy, R., & Haselgrove, J. H. (2001). Quantitative apparent diffusion coefficient measurements in term neonates for early detection of hypoxic-ischemic brain injury: Initial experience. *Radiology*, 218(3), 825–833.
- Zhai, G., Lin, W., Wilber, K. P., Gerig, G., & Gilmore, J. H. (2003). Comparisons of regional white matter diffusion in healthy neonates and adults performed with a 3.0-T head-only MR imaging unit. *Radiology*, 229(3), 673–681.

SUPPORTING INFORMATION

Additional supporting information may be found in the online version of the article at the publisher's website.

How to cite this article: Bobba, P. S., Weber, C. F., Mak, A., Mozayan, A., Malhotra, A., Sheth, K. N., Taylor, S. N., Vossough, A., Grant, P. E., Scheinost, D., Constable, R. T., Ment, L. R., & Payabvash, S. (2022). Age-related topographic map of magnetic resonance diffusion metrics in neonatal brains. *Human Brain Mapping*, 43(14), 4326–4334. <https://doi.org/10.1002/hbm.25956>